



A multiscale model for multiple platelet aggregation in shear flow

Prachi Gupta¹ · Peng Zhang^{1,2} · Jawaad Sheriff² · Danny Bluestein² · Yuefan Deng¹

Received: 21 June 2020 / Accepted: 22 January 2021 / Published online: 29 March 2021
© The Author(s), under exclusive licence to Springer-Verlag GmbH Germany, part of Springer Nature 2021

Abstract

We developed a multiscale model for simulating aggregation of multiple, free-flowing platelets in low–intermediate shear viscous flow, in which aggregation is mediated by the interaction of $\alpha_{IIb}\beta_3$ receptors on the platelet membrane and fibrinogen (Fg). This multiscale model uses coarse grained molecular dynamics (CGMD) for platelets at the microscales and dissipative particle dynamics (DPD) for the shear flow at the macroscales, employing our hybrid aggregation force field for modeling molecular level receptor ligand bonds. We define an aggregation tensor and use it to quantify the molecular level contact characteristics between platelets in an aggregate. We perform numerical studies under different flow conditions for platelet doublets and triplets and evaluate the contact area, detaching force and minimum distance between different pairs of platelets in an aggregate. We also present the dynamics of applied stress and velocity magnitude distributions on the platelet membrane during aggregation and quantify the increase in stress in the contact region under different flow conditions. Integrating the knowledge from our previously validated models, together with new aggregation scenarios, our model can dynamically quantify aggregation characteristics and map stress and velocity distribution on the platelet membrane which are difficult to measure in vitro, thus providing an insight into mechanotransduction bond formation response of platelets to flow-induced shear stresses. This modeling framework, together with the tensor method for quantifying inter-platelet contact, can be extended to simulate and analyze larger aggregates and their adhesive properties.

Keywords Multiscale modeling · Free-flowing aggregation · Aggregation tensor · Contact area · Stress distribution

1 Introduction

Cardiovascular diseases pose an immense health and economic burden in the USA (Benjamin et al. 2019) and the world. Presently, an estimated 18.2 million patients suffer from coronary heart disease in the USA and though the advent of cardiovascular devices has provided life-saving solutions to millions of these patients (De Lazzari et al. 1998; Guezuraga and Steinbring 2004), they have increased the thromboembolic risk requiring lifelong antithrombotic drug therapy in such individuals. Platelet aggregation in response to biochemical mechanisms and mechanical stimuli lead to thrombus and thromboembolic formation that can occlude vasculature and cause life-threatening vascular

diseases. Antiplatelet drug therapy currently overlooks the role of shear-induced platelet aggregation mediated via mechanotransduction (Slepian et al. 2017). Shear-induced platelet aggregation can stimulate blood clotting alone by exposing integrin $\alpha_{IIb}\beta_3$ on the platelet membrane (Harker and Slichter 1970; O'Brien 1990; O'Brien and Salmon 1989), making it increasingly important to investigate the role of mechanical stimuli and to seek more effective therapy than inhibition of biochemical pathways.

When a thrombus is formed, it creates discrete zones of spatially varying shear stress where the leading edge and the downstream region of the thrombus experiences low shear stress like that in regions of free flow, whereas the sides of the thrombus in the direction of flow there are regions of higher shear (Nesbitt et al. 2009). In the absence of soluble agonists (like ADP and thrombin), shear microgradient-induced discoid platelet aggregates are formed (Nesbitt et al. 2009). Platelet thrombi or aggregates have been observed in our in vitro studies (Gupta et al. 2019) and also in the post-stenotic region of atherosclerotic plaques (Falk 1985; Jackson et al. 2009). At venous shear rates (low shear), platelet

✉ Yuefan Deng
Yuefan.Deng@StonyBrook.edu

¹ Department of Applied Mathematics and Statistics, Stony Brook University, Stony Brook, NY 11794, USA

² Department of Biomedical Engineering, Stony Brook University, Stony Brook, NY 11794, USA

aggregation in free flow occurs through $\alpha_{\text{IIb}}\beta_3$ -Fg binding without the need of vWF (Brass and Diamond 2016; Sheriff and Bluestein 2019).

Platelet aggregation in free flow is a dynamic process that requires multiscale modeling techniques to capture the microscopic responses of the platelet to the macroscopic mechanical stimuli from the shear flow. This becomes increasingly important as the role of external mechanical forces on platelets is investigated for drug therapy. Platelet aggregation in free-flowing platelets may occur independent of adhesion, in which case the platelet forms small aggregates that can travel to other sites preventing blood flow. Platelet aggregates formed in low shear through the activation of integrin $\alpha_{\text{IIb}}\beta_3$ are stable (Nesbitt et al. 2009).

Several computational models (Mody and King 2008a, 2008b; Pivkin et al. 2006; Shiozaki et al. 2016; Tosenberger et al. 2012a, 2012b; Yazdani et al. 2017, 2018) have modeled aggregation and thrombus formation. Platelet adhesive dynamics (PAD) (Mody and King 2008a, 2008b) studies transient platelet aggregation in unactivated platelets through platelet integrin GPIIb α and the von Willebrand factor (vWF). The modeling technique combines a Monte Carlo simulation of GPIIb α -vWF binding with hydrodynamic calculations using the boundary integral method. Platelets are modeled as rigid oblate spheroids, while inter-platelet collisions are quantified using collision time, contact area and collision efficiency. In addition, the effect of the wall on the collisions and comparison with spherical particle collisions are studied. Molecular dynamics was used (Shiozaki et al. 2016) to predict the structure of vWF binding to GPIIb α for modeling platelet adhesion. A force coupling method (FCM) (Pivkin et al. 2006) was used to simulate platelet aggregation in a straight tube and investigate the effect of blood flow pulsatility. Yazdani et al. (Yazdani et al. 2017) developed a shear-dependent thrombus formation model using a coupled Eulerian-Lagrangian model where FCM is used to describe the interactions between flow and platelets, which are described as Lagrangian particles, and hemodynamics is solved on a fixed Eulerian grid using the spectral element method. These models fail to capture the multiscale interactions of platelets, which must undergo physiological changes in response to mechanical signals.

We have made considerable effort toward constructing a multiscale platelet model in blood plasma flow and using it for modeling aggregation. The macroscopic properties of blood plasma flow are modeled using dissipative particle dynamics (DPD), and coarse-grained molecular dynamics (CGMD) is used to model deformable platelets with the intracellular constituents at microscales. For this, a spatial interface was established between platelet membrane and flow by constructing a hybrid force field (Zhang et al. 2014b). A no-slip boundary condition was established between the flow and boundary (Soares et al. 2013), and

a modified Morse potential was developed for simulating the cytoplasm (Zhang et al. 2014a). In (Zhang et al. 2017), a platelet model with 140,015 particles validated the intra-platelet components (consisting of the bilayer platelet membrane, gel-like cytoplasm and intra-platelet cytoskeleton) properties with the published in vitro studies and continuously changes its morphology in response to the dynamic flow stresses (Zhang et al. 2014b, 2017). We used this multiscale platelet model to model recruitment aggregation in low shear stress mediated through the binding of $\alpha_{\text{IIb}}\beta_3$ and fibrinogen (Fg) (Gupta et al. 2019). In this approach, one platelet is adhered to the vessel wall and a flowing platelet in blood plasma is recruited to the adhered platelet. We validated the hybrid inter-platelet aggregation force field with our in vitro studies and also elucidated the role of platelet deformability during the aggregation process.

One of the hallmarks of some cardiovascular disease processes and blood recirculating devices is that those may potentiate thromboembolic complications by dissemination of free emboli in distal organs. Understanding the dynamics of platelet aggregation mediated by integrin $\alpha_{\text{IIb}}\beta_3$ can help design potential pharmacological approaches targeted to destabilize the platelet aggregates and therefore prevent clot formation. There is a paucity of literature regarding their formation, and simulations of such free emboli are very scant as computational efforts mostly deal with platelet-wall interactions. The goal of this work is to study the adhesive nature of free-flowing aggregation involving multiple discoid platelets in low-intermediate shear flow while also investigating mechanical properties that the aggregate experiences due to aggregation under shear flow. We simulate platelet aggregation in free flow under low-intermediate shear flow, independent of adhesion and visible shape change. We use our hybrid aggregation force field (Gupta et al. 2019) to model receptor-ligand bond between platelets and predict aggregate properties for three platelets.

The capability of our model to characterize molecular level mechanotransduction of hemodynamic stresses enables us to present dynamic mapping of stress distribution on the platelet membrane in the aggregate. We also present the stress in the contact region and show how contact and bond formation leads to an increase in localized stress. The velocity magnitude distribution is mapped on to the platelet surface and shows fluidity of the platelet membrane. The contact area and detaching force are also measured from the simulations for both rotation and translation and demonstrate the effect of flow on the aggregate. The molecular level bonding and debonding details and the root mean square fluctuation (RMSF) of the platelet aggregates are also presented.

2 Methods

2.1 Multiscale modeling for platelet aggregation

To overcome the limitation of continuum-based approaches in bridging the gap between macroscopic flow scales and the cellular scales characterizing platelet interaction with blood flow, the platelet aggregation was modeled using a multiscale model that uses DPD for simulating the top scale macroscopic shear flow and CGMD for the bottom molecular scale platelets (Gao et al. 2017; Zhang et al. 2014b, 2017), and a hybrid force field for aggregation between platelets (Gupta et al. 2019). Each DPD particle represents a cluster of atoms or molecules and their collective motion is governed by following (Español and Warren 1995; Groot and Warren 1997):

$$dv_i = \frac{1}{m_i} \sum_{j \neq i}^N (F_i^C dt + F_i^D dt + F_i^R \sqrt{dt} + F_i^E dt) \tag{1}$$

where $F_i^C = \alpha \left(1.0 - \frac{r_{ij}}{r_c}\right) e_{ij}$, $F_{ij}^D = -\gamma \omega^D(r_{ij}) (e_{ij} \cdot v_{ij}) e_{ij}$, $F_{ij}^R = \sigma \omega^R(r_{ij}) \zeta_{ij} e_{ij}$, $\omega^D(r_{ij}) = [\omega^R(r_{ij})]^2 = \left(1.0 - \frac{r_{ij}}{r_c}\right)^{2k}$. The F^C, F^D, F^R are conservative, dissipative and random forces acting on the particle and F^E is the external force exerted to each particle to lead the fluid flow. r_{ij} is the interparticle distance, $v_{ij} = v_i - v_j$ is the relative velocity and e_{ij} is a unit vector in the direction $r_i - r_j$. ζ_{ij} is a Gaussian random variable with zero mean and unit variance. α is the maximum inter-particle repulsion given by $\alpha = 75k_b T / (\rho_f r_c)$ where ρ_f is the number of fluid particles. γ and σ are coefficients that determine the strength of the dissipative and random forces. Español et al. (Español and Warren 1995) established a relation between γ and σ and weight functions given by $\sigma^2 = 2\gamma k_b T$, $k_b T = 1.0$.

The DPD method with parameters $\alpha = 25.0$, $\gamma = 67.5$, $k = 0.25$, $r_c = 1.7$ (Gao et al. 2017) is used to model wall-driven viscous shear flow in straight microchannel of dimensions $16 \times 16 \times 12.4 \mu\text{m}$. The dynamic viscosity of the flow is $1.07 \text{ mPa} \cdot \text{s}$. Periodic boundary conditions are implemented in x and z dimensions. In the y dimension, a no-slip boundary condition between the flow and the vessel wall is imposed as previously described by (Soares et al. 2013). This general no-slip condition consists of the generation of fictitious particles by reflecting flow particles across the vessel wall (constructed with triangular plane) with inverted velocity to develop an equilibrated shear layer across the microchannel wall, thereby imposing zero velocities at the wall plane (Soares et al. 2013; Willemsen et al. 2000).

The particle-based molecular scale deformable platelet model consisting of the bilayer membrane, cytoskeleton and cytoplasm employs CGMD potential given by

$$V_{\text{CGMD}} = \sum_{\text{bonds}} k_b (r - r_0)^2 + \sum_{L-J} 4\epsilon_{ij} \left[\left(\frac{\sigma_{ij}}{r}\right)^{12} - \left(\frac{\sigma_{ij}}{r}\right)^6 \right] \tag{2}$$

where k_b is the force constant, r_0 is the equilibrium distance, ϵ_{ij} is the well depth of the Lennard-Jones (L-J) potential, σ_{ij} is the finite distance and r is the interparticle distance (Zhang et al. 2014b). The first term in Eq. (2) describes the deformability of the membrane (Lakes 2001), and the second term describes the interaction between membrane and the intracellular particles (Zhang et al. 2017). Young’s modulus for our membrane is $(1.5 \pm 0.6) \times 10^3 \text{ dyne/cm}^2$ (Zhang et al. 2014b). In vitro, Young’s modulus for resting human platelets is $(1.7 \pm 0.6) \times 10^3 \text{ dyne/cm}^2$ (Haga et al. 1998).

The DPD–CGMD methods are spatially interfaced at the platelet membrane surface using the following hybrid force field (Zhang et al. 2014b)

$$dv_i = \frac{1}{m_i} \sum_{j \neq i}^N \left(\nabla U_{LJ}(r_{ij}) dt + F_{ij}^D \sqrt{dt} + F_{ij}^R dt \right) \tag{3}$$

where $F_{ij}^D = -\gamma \omega^D(r_{ij}) (e_{ij} \cdot v_{ij}) e_{ij}$, $F_{ij}^R = \sigma \omega^R(r_{ij}) \zeta_{ij} e_{ij}$ where ϵ and σ are the characteristic energy and distance parameters in CGMD. Other parameters including γ and σ have the same definitions as in DPD. All forces are truncated beyond a cut-off radius which defines the length scale in the fluid–platelet contact region (Fedosov and Karniadakis 2009).

The L-J potential maintains the cytoskeleton-confined shapes and the incompressibility of the platelets against the applied stress of the flow; dissipative and random force terms model interactions between the flow and platelet, thus preserving local thermodynamic and mechanical properties; and the repulsive drag force imposes no slip on the platelet membrane. The dissipative forces of the membrane particles drag the flow particles, thereby reproducing boundary layer mechanism where adjacent layers are dragged by one and the L-J potential provides a repulsive force preventing the flow particles from penetrating through the platelet membrane. The interaction between the two systems preserves dynamic properties of the flowing platelets, such as the flipping motion (Zhang et al. 2014b). This deformable platelet model is immersed in a DPD fluid in which the microstructural changes of platelets respond to the extracellular viscous shear stresses transferred to them and can therefore be used for modeling platelet aggregation in free flow.

In this work, we study aggregation of free-flowing platelets under constant shear stress through $\alpha_{\text{IIb}}\beta_3$ -mediated binding of Fg. There are 80,000–100,000 $\alpha_{\text{IIb}}\beta_3$ receptors on a typical platelet surface (Michelson 2013) that serve as a physical connector between fibrinogen and the platelet cytoskeleton (Jackson 2007; Maxwell et al. 2007; Qiu et al.

2015). We follow (Gupta et al. 2019) for the aggregation force field given by:

$$F_{ij} = \left(2\alpha D_0 \left(e^{-2\alpha(r_{ij}-r_0)} - e^{-\alpha(r_{ij}-r_0)} \right) + f^A \left(1 - \frac{r_{ij}}{r_0} \right) \right) \mathbf{e}_{ij} \tag{4}$$

where r is the distance between two particles and r_0 is the equilibrium bond length, D_0 is the well depth, α is the scaling factor, r_0 is the equilibrium bond length $\mathbf{r}_{ij} = \mathbf{r}_i - \mathbf{r}_j$, $r_{ij} = |\mathbf{r}_{ij}|$, $\mathbf{e}_{ij} = \mathbf{r}_{ij}/r_{ij}$ and f^A is the force strength coefficient. The Morse term in the force field consists of (i) an attractive part ($-e^{-\alpha(r_{ij}-r_0)}$) that contributes to aggregation by initiating and enhancing bond formation and (ii) a repulsive part ($e^{-2\alpha(r_{ij}-r_0)}$) that prevents the membrane particles from overlapping during aggregation. The parameter r_0 represents the force relaxation distance, F_{ij} is repulsive when $r_{ij} < r_0$ and attractive when $r_{ij} > r_0$.

In low–intermediate shear flows, aggregation requires $\alpha_{Iib}\beta_3$ and ligand Fg binding and can occur independent of shape change (Maxwell et al. 2007). Each platelet includes 67,004 $\alpha_{Iib}\beta_3$ receptors (Michelson 2013) represented by particles and distributed uniformly on the membrane. Receptor density on the platelet surface is 2342 particles/ μm^2 . To adapt the force field Eq. 4 for modeling aggregation at microscales, we use the bond length of $r_0 = 0.38$, which is the equilibrium bond length of $\alpha_{Iib}\beta_3$ -Fg- $\alpha_{Iib}\beta_3$ (67.5 nm) (Goldsmith et al. 2000) in dimensionless units. The approximate distance between the platelet surface that allows for bond formation was used to determine the cutoff (r_c). The $\alpha_{Iib}\beta_3$ receptors extend about 20 nm above the surface (Parise and Phillips 1985; Weisel et al. 1992), and Fg is about 47.5 nm in molecular length (Liang et al. 2010). The approximate distance between platelet surfaces for aggregation to begin is 87.5 nm. The undetermined parameters α , D_0 and f^A (Gupta et al. 2019), which determine the aggregation force between the two platelets, were determined by correlating with contact area (coarse-grained tuning) measured from the in vitro images and detaching force (fine grained tuning) obtained from AFM measurements (Litvinov et al. 2016). Figure 1 presents the details of the aggregation model. We simulate aggregation under different flow conditions: (a) Couette flow with rotation and (b) Couette flow with translation in shear 10 dyne/cm². The details of our simulations are described in Fig. 2 and Sect. 2.3.

2.2 Measures and formulae

Platelet aggregation can be quantified using (i) contact area, (ii) detaching force, (iii) nearest distance and (iv) center distance. Additionally, we can evaluate the mechanical properties of the aggregate like (i) stress and (ii) velocity magnitude. In this section, these quantities are defined and

algorithms for averaging microscopic quantities to obtain macroscopic trends are presented.

The center distance refers to the distance between the centers of mass of two platelets and is calculated as $x = \|\mathbf{r}_A - \mathbf{r}_B\|_2$, where \mathbf{r}_A and \mathbf{r}_B are the centers of mass for platelets A and B, respectively. To calculate the nearest distance, r_{ij} is computed between the i^{th} particle on membrane platelet A and j^{th} particle on membrane of platelet B,

$$d_{min} = \min \left\{ r_{ij} | r_{ij} = \|\mathbf{r}_i - \mathbf{r}_j\|, \mathbf{r}_i \in M_A, \mathbf{r}_j \in M_B \right\} \tag{5}$$

where M_A and M_B are the group of membrane particles for platelets A and B, respectively.

We define the set of contact particles as:

$$C_{AB} = \left\{ r_i | r_{ij} < T_d, r_{ij} = \|\mathbf{r}_i - \mathbf{r}_j\|, \mathbf{r}_i \in M_A, \mathbf{r}_j \in M_B \right\} \tag{6}$$

where $T_d = 87.5$ nm (Gupta et al. 2019). Hence, contact area is defined as:

$$C_a = |C_{AB}| \cdot \frac{S}{|M|} \tag{7}$$

where S is the surface area and M is the set of membrane particles of the platelet where $|\cdot|$ is the notation for cardinality of a set. The detaching force is calculated as multiples of the rupture force for $\alpha_{Iib}\beta_3$ and Fg bonds approximate number of $\alpha_{Iib}\beta_3$ -Fg bonds. Since aggregation is a dynamic phenomenon, we use RMSF to analyze differences in trajectory that arise from rigidity or deformability of the platelets and determine a stable state for aggregation. Specifically, RMSF is used to determine an average position about which the system may possess some small fluctuations. We calculate RMSF by the following formula:

$$RMSF(\Delta t) = \sqrt{\frac{1}{N} \sum_{i=1}^N (r_i(t + \Delta t) - r_i(t))^2} \tag{8}$$

where N is the number of particles and $r_i(t)$ is the position of particle i at time t .

The properties of stress and velocity magnitude measured from the simulations for membrane particles are instantaneous and possess instantaneous fluctuations; thus, their direct use to illustrate the stress and velocity patterns on platelet membranes is inadequate. Per atom virial stress does not have a direct physical interpretation, but these provide a means for grouping contributions together to allow an estimation for spatial variation of stress tensor (Heinz et al. 2005; Thompson et al. 2009). To obtain a more meaningful trend of them, we perform temporal and spatial averaging, with calculated window sizes. For this, we follow three steps: (i) convert from tensor/vector to scalar, (ii) temporal averaging and (iii) spatial averaging.

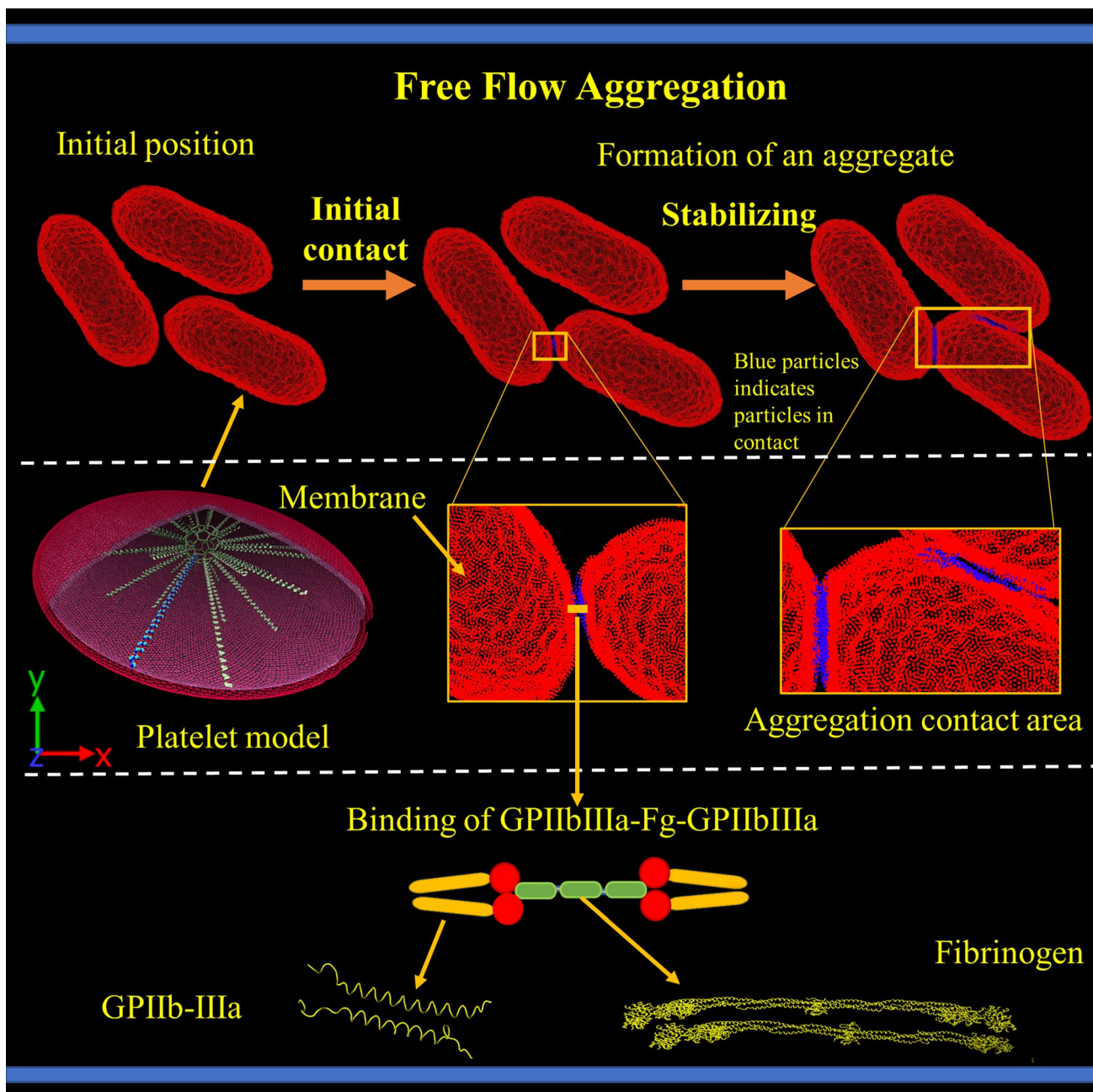


Fig. 1 Schematic representation of the platelet aggregation model

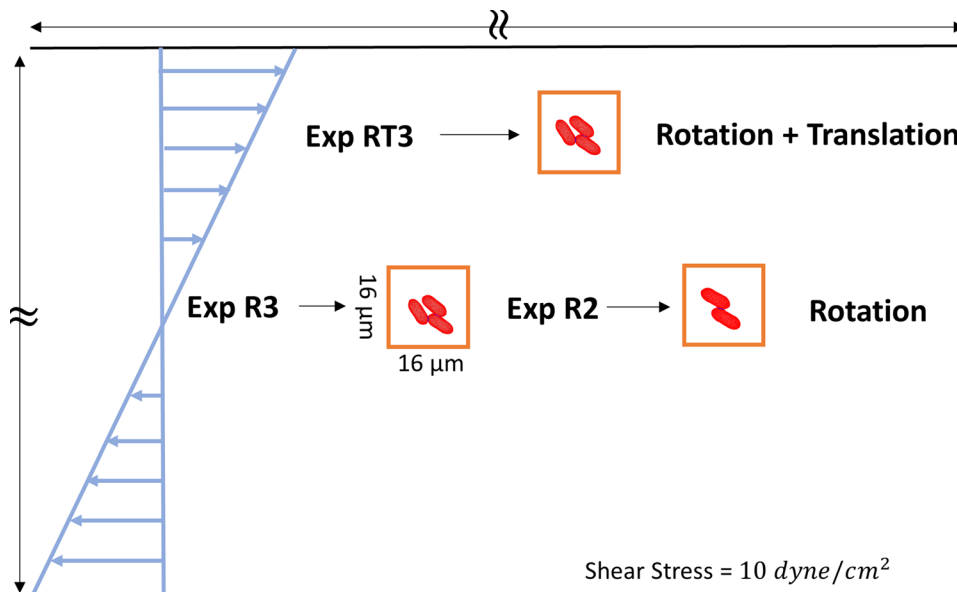
Step 1 The virial theorem computes the volume-averaged stress tensor for a group of particles (Heinz et al. 2005; Thompson et al. 2009). To render the stress tensor to a scalar, we use the following formulation (Alemu and Bluestein 2007; Apel et al. 2001):

$$\hat{\tau}(p, t) = \frac{1}{\sqrt{3}} \sqrt{\tau_{xx}^2 + \tau_{yy}^2 + \tau_{zz}^2 - \tau_{xx}\tau_{yy} - \tau_{xx}\tau_{zz} - \tau_{yy}\tau_{zz} + 3(\tau_{xy}^2 + \tau_{yz}^2 + \tau_{xz}^2)}$$

for a membrane particle p at time t . To compute the velocity magnitude for the particles, we use:

$$\| \mathbf{v}(p, t) \|_2 = \sqrt{v_x^2 + v_y^2 + v_z^2}$$

Fig. 2 Schematic representation of simulations. R2 denotes the simulation for platelet doublets and R3 for platelet triplets along the center line of the microchannel. RT3 denotes the simulation for platelet triplets closer to the boundary. For each simulation, the dimensions of the microchannel are length (L) 16 μm, height (H) 12.4 μm and width (W) 16.0 μm



for a membrane particle p at time t .

Step 2 Temporally, we average consecutive instantaneous properties over a finite time period. For example, temporal averaging of time follows the following:

$$\langle \hat{\tau}_{\text{time}} \rangle = \frac{1}{n} \sum_{j=0}^{n-1} \hat{\tau}_k(j \cdot \Delta t) \tag{11}$$

Step 3 For mitigating fluctuations due to membrane deformability, spatial averaging technique is employed to average over a surface volume of platelet membrane as follows:

$$\bar{\tau}_k = \frac{1}{M} \sum_{r_k \in D(p, \delta)} \langle \hat{\tau}_{\text{time}} \rangle \tag{12}$$

where r_k is a particle of membrane, $D(p, \delta)$ represents the δ -neighborhood of particle p , $M = |D(p, \delta) \cap \{r_k\}|$. The temporal averaging is done for 200,000 time steps (20 μs) and the spatial averaging $\delta^2 = 1.2$.

2.3 Aggregation tensor

Thrombus formation involves multiple platelets and their aggregation characteristics change dynamically over time. Since tensors provide a more natural representation of complex dynamical quantities, we utilize tensors to develop a framework for analyzing aggregation characteristics. In this section, we outline the framework for n platelet systems that may have multiple aggregates of different sizes and provide examples to illustrate the use of this framework. Section 2.4 presents the details of numerical experiments setup for two and three platelet aggregates,

and in Sect. 3, we analyze and present detailed results for aggregation properties measured from the simulations.

Definition 2.1 Let $a_{ij}(t), i \neq j$, denote the contact area between platelets p_i and p_j at time t , where $a_{ij} = a_{ji}$ and a_{ii} represent the surface area for the platelet p_i . The aggregation tensor A for n platelets, such that $A(t) \in \mathbb{R}^{n \times n} \forall t$ can be defined as follows:

$$A(t) = [a_{ij}(t)] = \begin{pmatrix} a_{11}(t) & \cdots & a_{1n}(t) \\ \vdots & \ddots & \vdots \\ a_{n1}(t) & \cdots & a_{nn}(t) \end{pmatrix}$$

This aggregation tensor represents the aggregation dynamics between platelets in the system using the contact area metric. When the aggregate formation has not started, the matrix $A(t)$ is reduced to a diagonal matrix. As the platelets begin to aggregate, off-diagonal entries become nonzero, and as more and more platelets attach themselves to the thrombus, the sparsity of the matrix decreases. For a fixed number of platelets (i.e., a fixed n) in the system, a dense matrix is indicative of a large number of contacts between platelets, and the number of nonzero entries indicates the number of platelets in the aggregate.

Definition 2.2 Let $a_{ij}(t), i \neq j$, denote the contact area between platelets p_i and p_j at time t , the norm is defined as $\|A\| = \sum_{i < j} |a_{ij}(t)|$.

The quantity $\|A\|$ denotes the total contact area of the aggregate and can be used as a measure of strength of the aggregate. An increase in the number of platelets and the contact area between the platelets leads to a larger value for $\|A\|$.

Definition 2.3 Let $c_{ij} = \begin{cases} 0, & i = j \text{ or } a_{ij} = 0 \\ 1, & \text{otherwise,} \end{cases}$ then the matrix contact matrix is defined as $C = [c_{ij}]$.

Definition 2.4 If $\Omega = \{p_k, p_l, p_m\}$ forms an aggregate, then the k -th, l -th, m -th row of the n -D identity matrix forms a selection matrix S such that SCS^T is the matrix representing the aggregate Ω .

Definition 2.5 The rate of change of tensor A is defined as:

$$\frac{\Delta A}{\Delta t} = \frac{a_{ij}(t + \Delta t) - a_{ij}(t)}{\Delta t} = \begin{pmatrix} \frac{a_{11}(t+\Delta t)-a_{11}(t)}{\Delta t} & \dots & \frac{a_{1n}(t+\Delta t)-a_{1n}(t)}{\Delta t} \\ \vdots & \ddots & \vdots \\ \frac{a_{n1}(t+\Delta t)-a_{n1}(t)}{\Delta t} & \dots & \frac{a_{nn}(t+\Delta t)-a_{nn}(t)}{\Delta t} \end{pmatrix}$$

For $i \neq j$, if $\frac{a_{ij}(t+\Delta t)-a_{ij}(t)}{\Delta t} < 0$, the debonding for that platelet pair occurs and a large number of negative tensor elements denote disaggregation. For $i = j$, if $\frac{a_{ij}(t+\Delta t)-a_{ij}(t)}{\Delta t} > 0$, surface area increases indicating platelet expansion, e.g., observed during aggregation or adhesion process. Thus, the tensor can measure the various phenomenological changes that platelets undergo during or after aggregate formation and can be quite useful for large aggregates.

Definition 2.6 Time integral of contact area is defined as follows:

$$\int_t^{t+t_w} A(t)dt = \sum_t^{t+t_w} a_{ij}(t)dt \quad \text{for } i, j = 1 \dots n$$

where $t_w = w \cdot dt$ is the window size for moving average.

This tensor demonstrates the trend in the contact area. This tensor helps to preserve the microscale and pairwise properties of the platelets in larger aggregate formation models which otherwise may get lost in coarse measurements like volume and growth rate. of the aggregate. The details of the algorithm for finding the number and size of aggregates are presented in Online Resource 1 (supplementary materials).

2.4 Numerical simulations

Figure 2 presents the simulations that were conducted for this study. We conduct the simulations in two flow regimes for two and three platelets (a) at the center of the microchannel (experiments R2, R3) and (b) closer to the boundary of the microchannel (experiment RT3). For each simulation, Couette flow was employed to model blood plasma in a microchannel of length (L) 16 μm , height (H)

12.4 μm and width (W) 16.0 μs . The number density for fluid is 3.0. Each platelet was modeled as an ellipsoid with dimension $4 \times 4 \times 1$ in μm (Zhang et al. 2017) and has 140,303 particles. This platelet model continuously changes its morphology in response to the dynamic flow stresses during aggregation. For each simulation, the microchannel has platelets placed at the center such that they are not in the aggregation interaction range of each other at the start of the simulation. The integration time step size reported is 2.5×10^{-5} (Table 1). We run the simulations until aggregation becomes stable, and there is no significant change in contact area. All simulations were performed with NVE ensemble, using LAMMPS (Large-scale Atomic/Molecular Massively Parallel Simulator) code (Plimpton et al. 2012), with added algorithms like no-slip boundary condition (Soares et al. 2013), DPD–CGMD hybrid potential for interactions between platelets and flow (Zhang et al. 2014b), hybrid DPD–Morse potential for reducing compressibility of the flow (Gao et al. 2017) and hybrid force field for modeling aggregation (Gupta et al. 2019). Platelet aggregation simulations presented in this manuscript take approximately a wall clock time of 2.81 h for 20,000 time steps (1.04 μs). Physical quantities in dimensionless units were converted into physical units for the interpretation of aggregation and flow properties. The wall shear stress is 10 dyne/cm², and shear rate is 932 s⁻¹ with a flow viscosity of 1.07 mPa · s. This shear stress level corresponds to the upper limit of the single-stage aggregation (~ 1000 s⁻¹) identified by the Jackson group (Jackson 2007; Maxwell et al. 2007). In this phase, aggregation is dominated by platelet integrin $\alpha_{\text{IIb}}\beta_3$ –Fg interactions. The model units are converted from dimensionless units to physical units (Zhang et al. 2017) (Table 1). The reference length $\sigma_r = \frac{D_\rho}{D_\rho^*}$, where $D_\rho = 4 \mu\text{m}$ and $D_\rho^* = 4$, the reference mass $m_r = \frac{\rho\sigma_r^3}{\rho^*}$ where the fluid density of blood plasma $\rho = 1060 \text{ kg/m}^3$ and the particle density $\rho^* = 3$. Aggregation tensor metrics are presented in Table 2. Reference units are presented in Table 3.

Table 1 Parameters for aggregation model

Key model parameters	Model values in DPD units	Model values in SI units
r_0	0.38	67.5nm
r_c	0.5	87.5 nm
α	1.0	5.62 μm^{-1}
D_0	10.0	1.45×10^{-19} J
f^A	10.0	0.82 pN
Δt	2.5×10^{-5}	52 ps

Table 2 Aggregation tensor metrics for analyzing aggregate properties

Key tensor metrics	Key biophysical properties
A	Aggregation tensor
$\frac{da_{ij}}{dt}, i \neq j$	Growth rate of contact area
$\frac{da_{ii}}{dt}$	Platelet spreading or shape change during activation
$\ A\ $	Total contact area for the aggregate
$\sum_t^{t+t_w} a_{ij}(t)dt$	Time integral of contact area

Table 3 Reference units used in the model for unit conversions from dimensionless to SI units

Terms	Symbol/formula	Model values	SI values	SI units
Length	σ_r	1	1.78×10^{-7}	m
Time	t_r	1	2.08×10^{-6}	s
Mass	m_r	1	1.99×10^{-18}	kg
Force	$\frac{m_r \sigma_r}{t_r^2}$	1	8.15×10^{-14}	N
Energy	$\frac{m_r \sigma_r^2}{t_r^2}$	1	1.45×10^{-20}	J
Velocity	$\frac{\sigma_r}{t_r}$	1	8.53×10^{-2}	m/s

3 Results

3.1 Contact area

Contact properties during platelet aggregation can be numerically quantified and analyzed through contact area and detaching force. Figure 3 shows platelet dynamics for the R3 setup leading to formation of an aggregate. Initially, the platelets are not within the interaction range of each other, but as the simulation proceeds, the flow pushes the platelets closer to each other within the interaction range, and the platelets start to aggregate. The blue color indicates the contact particles, i.e., the receptors, that have formed a bond. As the platelets continue to aggregate, we see that two pairs of platelets in the cluster aggregate.

We calculate the contact area from the numerical simulations for R3, RT3 and R2. The aggregation tensor A defined in Sect. 2.3 is used to describe and analyze the contact properties during aggregation. The evolution of contact area for each platelet pair and total contact area $\|A\|$ with the simulated time are presented in Fig. 4 for all three setups. For all setups, there is an initial rapid increase in contact area which indicates the formation of receptor ligand bonds. As the simulation proceeds, the contact area reaches a stable value indicating that the

formation of new bonds decreases, and the contact has stabilized. For the same initial platelet positions and the same number of platelets in contact, the total contact area $\|A\|$ is larger in R3 as compared to RT3 which shows the role of flow in influencing aggregation.

Online Resource 2 presents the growth rate of contact area and its trend using moving average for a_{13} and a_{23} , respectively. The raw data of growth rate show the fluctuation, which indicates bonding and debonding of receptor–ligands, and the trend line shows the nature of aggregation during that time. The peaks in the trend demonstrate periods of rapid bond formation leading to increase in contact area, whereas a flat line indicates stabilization. Supplementary S1 (last row) shows the time-averaged contact area that demonstrates the overall trend.

For the R3 setup, during the initial part of the simulations, we observe that there is rapid increase in contact area between platelets p1 and p3 for approximately the first 60 μ s followed by alternating small periods of stabilization and increase in contact area for the next 110 μ s, after which contact area is stable with small fluctuations. This can also be seen from the growth rate trend for a_{13} , which shows a large peak followed by two smaller peaks. For platelets p2 and p3, the contact area curve shows a uniform increase until a steady state is reached. The growth rate shows an initial peak followed by two smaller peaks. As the simulation proceeds, the peak growth rate decreases approaching 0 indicating no new bonds are formed.

For the RT3 setup, both contact areas experience similar trend of a rapid increase in the contact area in the first 75 μ s and then a stabilization of the contact area with small fluctuations. For platelets p1 and p3, the growth rate shows a large peak between two smaller peaks indicating that rapid increase in contact occurs between 50 and 60 μ s, whereas for p_2 and p_3 , the growth rate possesses several peaks all with the similar peak growth rate. This difference in growth of contact area over time demonstrates the role of flow and orientation in the aggregation process.

3.2 Stress distribution on the aggregate

The multiscale model for aggregation of multiple platelets generates massive amounts of data at the microscale for the measured physical properties. Our goal is to extract the macroscopic trend in these properties using spatial and temporal averaging techniques to present the dynamics that the aggregate undergoes. The stress tensor is rendered into scalar values for each membrane particle and averaged over time and volume following the methodology outlined in Sect. 3.2. Figure 5 (for movie see Online Resource 3), Online Resource 4 and Online Resource 5 present the dynamic stress distribution map on the platelet membrane for the aggregate for numerical experiments R3, RT3 and

R2. As the simulation proceeds for each case, we see that all platelets develop regions of high stress around the periphery of the platelet. The deformable platelet membrane responds to extracellular hemodynamic stresses, which enables the model to illustrate these patterns which may be linked to peripheral changes during activation. The platelet pseudopodia, fingerlike structures that aid in stabilization of aggregates, have been observed to grow from the periphery (Michelson 2013).

For setup R3, the top and side views in Fig. 5 show that as the platelets aggregate, and the contact area increases, there is an increase in stress around the contact regions a_{13} and a_{23} . This stress increase in the contact region is indicated by the color map changing from green to red starting at the contact point and then eventually propagating to the nearby region. Figure 5b presents the stress distribution map on platelet p3, in which the color map indicating the intensity of stress initially demonstrates an increase in stress on the membrane particles in the contact region. In the beginning, as aggregation proceeds with formation of new bonds, stress increases and is later stabilized as the contact area reaches a constant value, indicating that the aggregation simulation has reached a stable state.

For RT3 (Online Resource 3), as the cluster translates with the flow, the platelets aggregate and regions of high shear stress appear on the platelet periphery and in the contact regions similar to the R3 setup. These spots grow in intensity and area as the simulation proceeds, and the stress map for the platelet p3 of the aggregate clearly shows the two contact regions exhibiting an increase in stress due to bond formation.

We measure the stress in the contact region by identifying the contact particles (Sect. 3.2) and then calculating the average stress on those particles. Figure 6 presents the average stress in the contact region for the R3, RT3 and R2 setup. We observe that for all experiments, stress in the contact region follows the same asymptotic trend, i.e., stress increases in the initial stages of aggregation and becomes stable at an elevated stress value once the platelets form a stable contact. This trend is similar to that observed for contact area, which also shows a rapid increase for the initial stage of aggregation due to bond formation, followed by stabilization.

3.3 Velocity magnitude distribution on the aggregate

Figure 7 (for movie see Online Resource 6), Online Resource 7 and Online Resource 8 present the velocity magnitude map on the platelet membrane for the R3, RT3 and R2 setups, respectively. There are areas of higher velocity magnitude on the aggregate indicated by the red color. These areas of higher velocity magnitude change

intensity and location on the aggregate, which is also shown more clearly in Supplementary Material S2. These indicate the fluidity within the platelet membrane which is enabled by our unconstrained deformable model.

Online Resource 9 compares the average velocity magnitude for the three setups. From the figure, we see that the average velocity magnitude fluctuates for all setups; however, for the RT3 setup the average velocity increases initially and fluctuates at a higher value as compared to R2 and R3, which is expected because of the translation motion in RT3 setup.

3.4 Detaching force, nearest distance and RMSF

Figure 8 presents the detaching force, nearest distance, center distance and RMSF. Detaching force is calculated as a multiple of rupture force per $\alpha_{IIb}\beta_3$ -Fg bond and number of bonds between platelets measured from the simulations. The evolution of detaching force with time is presented in Fig. 8(a) for all three setups. The fluctuations in the curves indicate the bonding and debonding that occurs between membrane particles through the receptor–ligand bond. The detaching force and contact area follow a similar trend since they are directly proportional to each other. Nearest distance (d_{\min}) and center distance x are calculated for each pair of platelets in the cluster. Figure 8(b) shows the evolution of d_{\min} with the simulated time. As the platelets in the cluster come close to each other, the nearest distance decreases and eventually falls below the threshold value, thereby forming an aggregate, after which the nearest distance possesses fluctuations indicating the bonding and debonding of receptor and ligand. Fig. 8(c) shows the center distance between the platelets in the aggregate for all setups. Figure 8(d) shows the RMSF for the platelets in the cluster calculated for all setups. From the figure, we observe that for R3 and R2, the RMSF for all platelets in the cluster decreases, reaching a stable value. For RT3, the RMSF increases, reaching a higher value because of the translation effect.

Figure 9 presents the detaching force vs. center distance for all three setups. We can see that as the platelets come closer and more bonds are formed, the center distance decreases as the detaching force increases. The following empirically fitted equation can be used to describe this relationship between center distance (x) and detaching force $f(x)$:

$$f(x) = f_0 * e^{-\left(\frac{x-x_0}{c_0}\right)^2} \quad (12)$$

The parameters (f_0 , x_0 and c_0) and error for each numerical simulation are presented in Table 4.

Table 4 Parameters for model describing the relationship between detaching force and center distance for all setups

Numerical simulations	f_0	x_0	c_0	R-square
R3_13	162.7	1.153	0.04560	0.989
R3_23	238.7	1.529	0.06187	0.994
RT3_13	300.0	1.137	0.04571	0.987
RT3_23	164.3	1.536	0.05761	0.989
R2	157.0	1.192	0.01656	0.986

3.5 Comparison of the numerical experiments

Figure 10(a) presents the comparison of stress distribution on the aggregates for all setups and in the contact region a_{13} for platelet p_3 and p_1 . For all aggregates, the stress distribution on the periphery of the platelets is different. Figure 10(b) compares the average stress in the contact region on platelet p_3 a_{13} along with detaching force, time-averaged contact in region a_{13} and total contact area. All metrics demonstrate asymptotic behavior and, in the region a_{13} , RT3 has the largest contact area and detaching force because of larger bond formation and hence larger stress in the contact region. However, the total contact area is greater in the case of R3, although R3 and RT3 have the same number of platelets in contact, demonstrating that the overall strength of R3 aggregate is larger.

4 Discussion

The multiple platelet aggregation model presented here studies the formation of an aggregate in viscous shear flow, and qualitatively and quantitatively examines the aggregate properties. For quantifying and analyzing the aggregation properties for multiple platelets, a tensor-based framework was designed. Using this multiscale model, we can compute the evolution of aggregation properties for an aggregate-like contact area, detaching force, nearest distance and RMSF. In addition, this platelet model can deform to model the microstructural changes of platelet constituents like the membrane, cytoplasm and cytoskeleton in response to the extracellular viscous shear stresses, thus describing mechanical properties like stress and velocity distribution on the aggregate.

Discoid, deformable platelets in free flow are simulated such that the platelets are initially not within the interaction range of the $\alpha_{IIb}\beta_3$ -Fg bond. The simulations are performed under constant shear for three and two platelet setups, respectively, in Couette flow with rotation and compared with a three-platelet simulation in Couette flow with translation. A hybrid force field using Morse and Hooke's force established in (Gupta et al. 2019) models aggregation between platelets as they are pushed by the flow into the bond formation range of the $\alpha_{IIb}\beta_3$ -Fg bond. For the first time, this high-resolution platelet aggregation model in flow can describe the molecular level bond formation during aggregation and can deform in response to the flow-induced

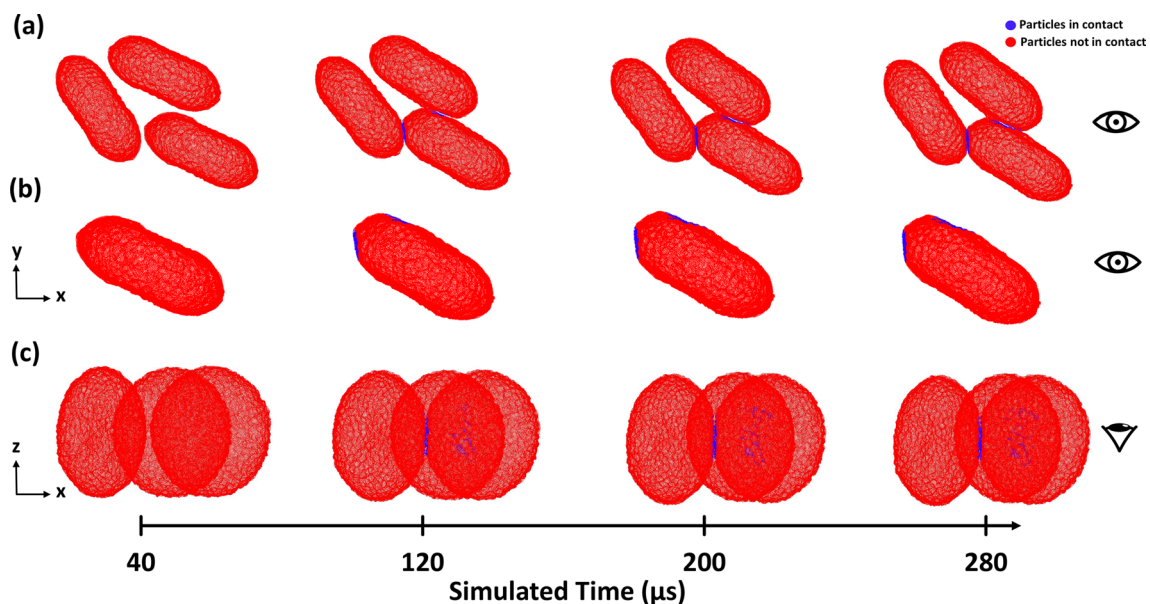


Fig. 3 Platelet aggregation dynamics for three platelets showing the contact area in the **a** side and **b** top view

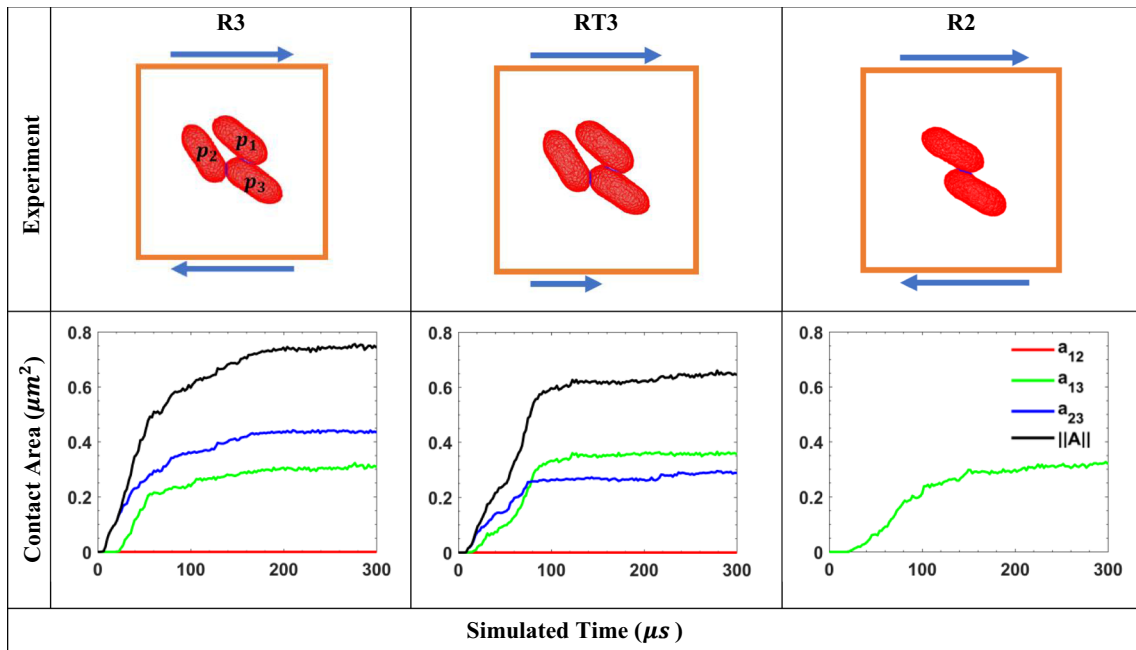


Fig. 4 Contact properties using the aggregation tensor

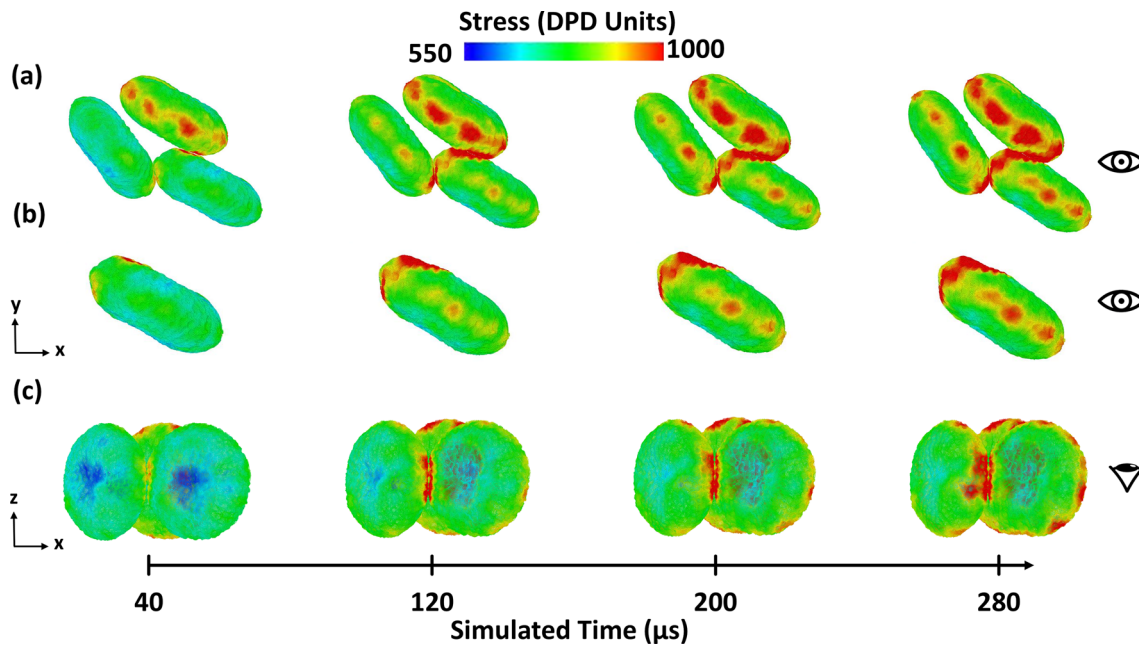


Fig. 5 **a** Top view of the stress distribution for the R3 simulation. **b** Stress distribution on contact regions of platelet p3 of the aggregate. **c** Front view of the stress distribution for the R3 simulation

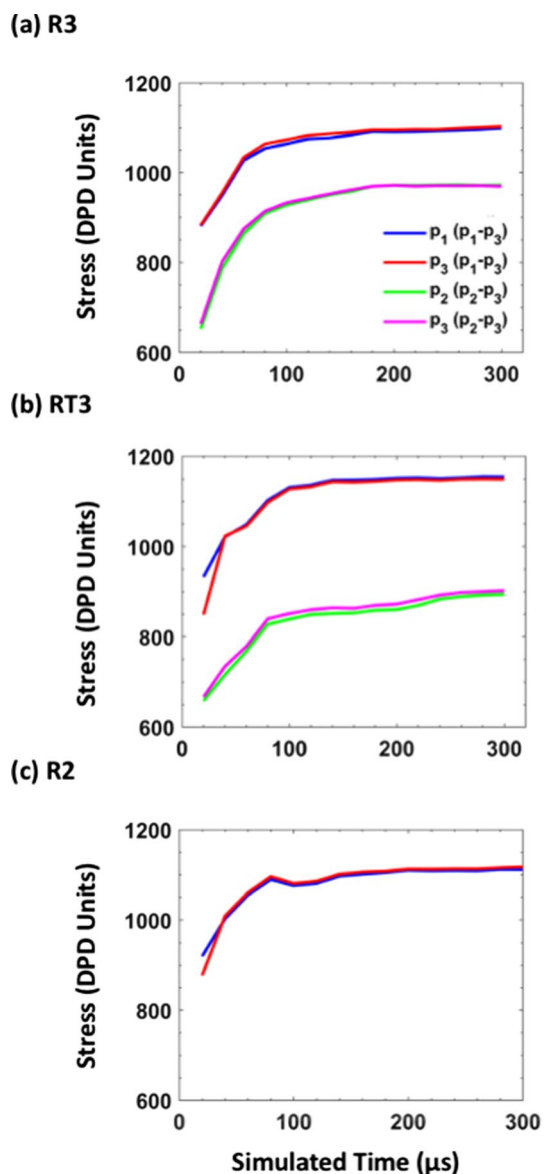


Fig. 6 Average stress in the contact region for simulations **a** R3, **b** RT3 and **c** R2

hemodynamic stresses, thus allowing study of stress distribution during aggregation.

Aggregation dynamics of the platelets for R3 and RT3 show that as the platelets are pushed closer to each

other by the flow, they begin aggregating and forming $\alpha_{IIb}\beta_3$ -Fg- $\alpha_{IIb}\beta_3$ bonds. As the simulations proceed, two pairs of platelets in contact show rapid increase in bond formation at first, leading to increase in contact area. After some time, the bond formation slows down, and contact area stabilizes, leading to formation of a stable aggregate. For RT3, this aggregate translates with the flow. The fluctuation in contact area and growth rate shows the microscale bond formation and disassociation activity during aggregation. The differences in evolution of aggregation dynamics are shown through how growth rates for the three simulations have different number and value for the peaks.

Several in vitro studies (Obrien 1990; Obrien and Salmon 1989) have investigated the role of shearing forces on activation of platelet receptors which initiate the aggregation response from platelets. However, it is not possible to study the dynamic distribution of the stress on the platelet membrane in vitro. We employ the computational model to qualitatively elucidate the stress distribution on the aggregate surface. The stress tensor at the microscale is converted to a scalar, and spatially and temporally averaged to present the distribution at the macroscale. As the platelets aggregated, we observed an increase in stress on the aggregate and regions of high shear stress around the periphery of the platelets. The deformable platelet membrane responds to extracellular hemodynamic stresses, which enables the model to illustrate these patterns and may be linked to peripheral changes during activation. The platelet filopodia, fingerlike structures that aid in stabilization of aggregates, have been observed to grow from the periphery (Michelson 2013; Sheriff and Bluestein 2019). Below the phospholipid bilayer membrane and at the periphery of the cytoskeleton, compressed spectrin-rich membrane networks are interlocked with binding protein complexes that connect to radially projected filamentous actin originating from the actin cortex at the core (Hartwig and Desisto 1991). The evolution of stress distribution in the contact region presented in this work shows that bond formation results in an increase in stress which quickly spreads to the nearby regions and that the stress increases with the increase in contact area.

The velocity magnitude distribution is presented for the aggregate, and we observe areas of higher velocity magnitude that change location and intensity as the simulation proceeds. These fluctuations in velocity magnitude are enabled

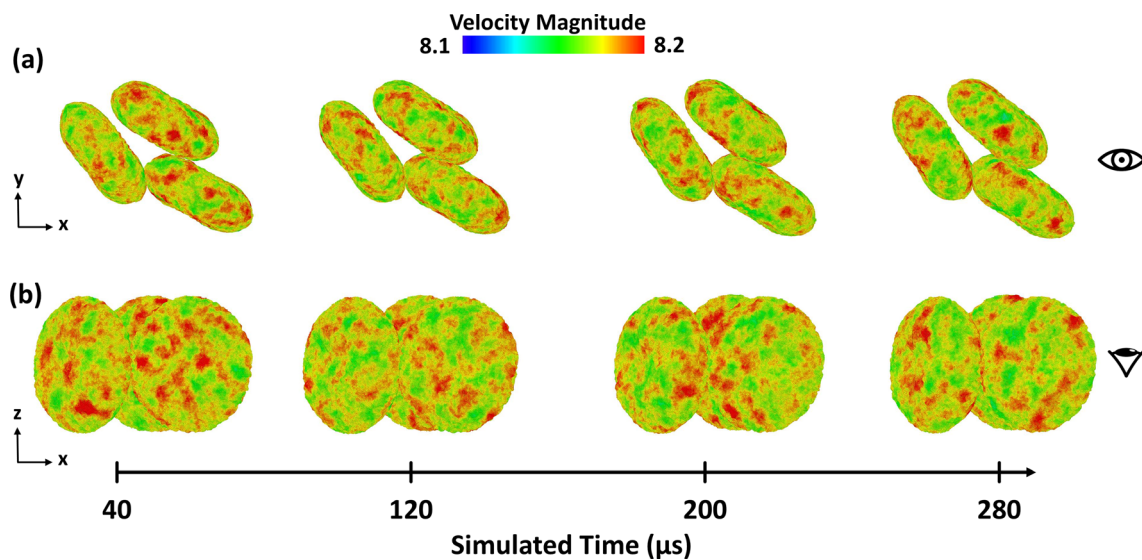


Fig. 7 Velocity magnitude distribution on the platelet membrane for the R3 setup in the **a** side and **b** top views

by our unconstrained deformable platelet model, which allows motion of particles relative to each other due to forces from the surrounding DPD flow and between adjacent membrane particles. Biologically, these may mimic fluidity of the membrane in response to biochemical agents (Watala et al. 1998), in which constitutive lipids can spatially rearrange and laterally diffuse (Slepian et al. 2017). These constitutive elements, which include specialized lipids and "lipid rafts," may act as mechanosensors that trigger platelet activation (Slepian et al. 2017), and variations in the membrane fluidity may modulate shear stress-driven mechanochemical signal transduction (Los and Murata 2004) responsible for events such as activation, aggregation and adhesion. Membrane fluidity allows rapid deflection of otherwise stiffly anchored transmembrane proteins, the classical mechanosensors and transducers (Slepian et al. 2017). Limited data suggest that exposure to 70 dyne/cm² for 10 min (stress accumulation of 42,000 dyne-s/cm²) leads to 6% increase in membrane fluidity, as determined by fluorescence anisotropy (Sweedo et al. 2020). These observations can be accommodated into a more advanced model to study the role and effect of lipids during aggregation. We aim to link observations of velocity fluctuations in our simulations to in vitro measurement of membrane element motion under shear stress exposure once a technique is identified for the latter.

The molecular effects of platelet aggregation can also be observed from the detaching force, nearest distance and

center distance. The nearest distance shows that none of the platelets are initially in contact, but as the simulation proceeds, two pairs of platelets contact and the nearest distance then fluctuates below the threshold distance, demonstrating bonding and debonding leading to a stable aggregate. The detaching force and center distance relationship was explored, showing an increase in detaching force as the center distance increases, and is modeled by a Gaussian fit. Comparing the setups R3, RT3 and R2, we observe that the contact area for different pairs of platelets in the aggregate is different for different setups. From the dynamics of stress, it also shows the difference in stress patterns on the platelets in the aggregate.

In this work, we present comprehensive numerical simulations for free-flowing aggregation. However, given the complexity of the platelet aggregation and the variety of factors that initiate and influence the aggregation process, our study has some limitations. This multiscale model assumes that integrin $\alpha_{IIb}\beta_3$ receptors interacting with Fg are distributed homogeneously throughout the membrane. In addition, simulations were performed under low–intermediate shear conditions, where aggregation without shape change has been observed and excludes shear conditions mediating aggregation via pseudopods. These assumptions reduce computational cost. Nevertheless, these assumptions are valid for platelets in the initial stage of activation where membrane receptors are actively expressed preceding

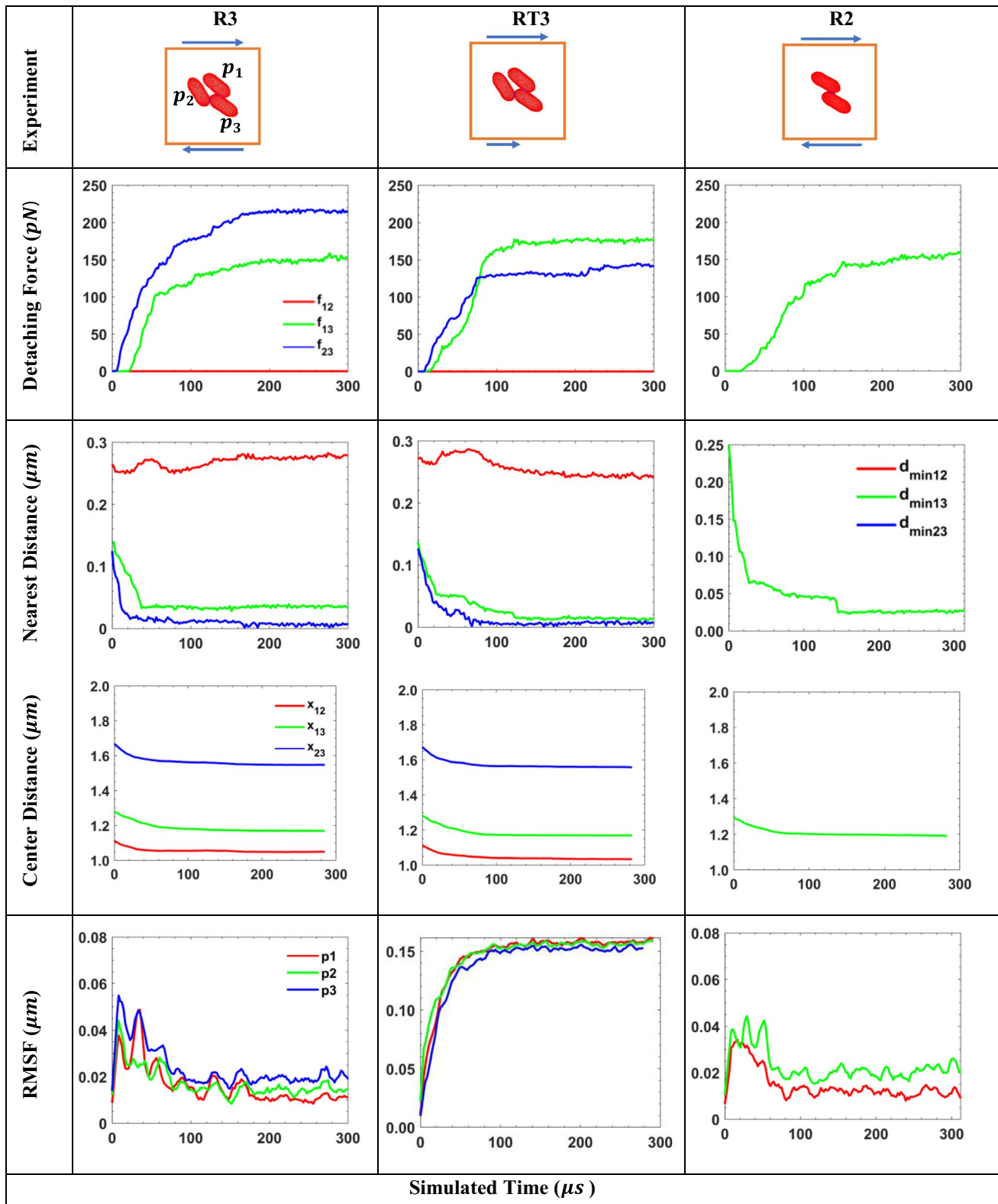


Fig. 8 Detaching force, nearest distance, center distance and RMSF during aggregation for all numerical simulations

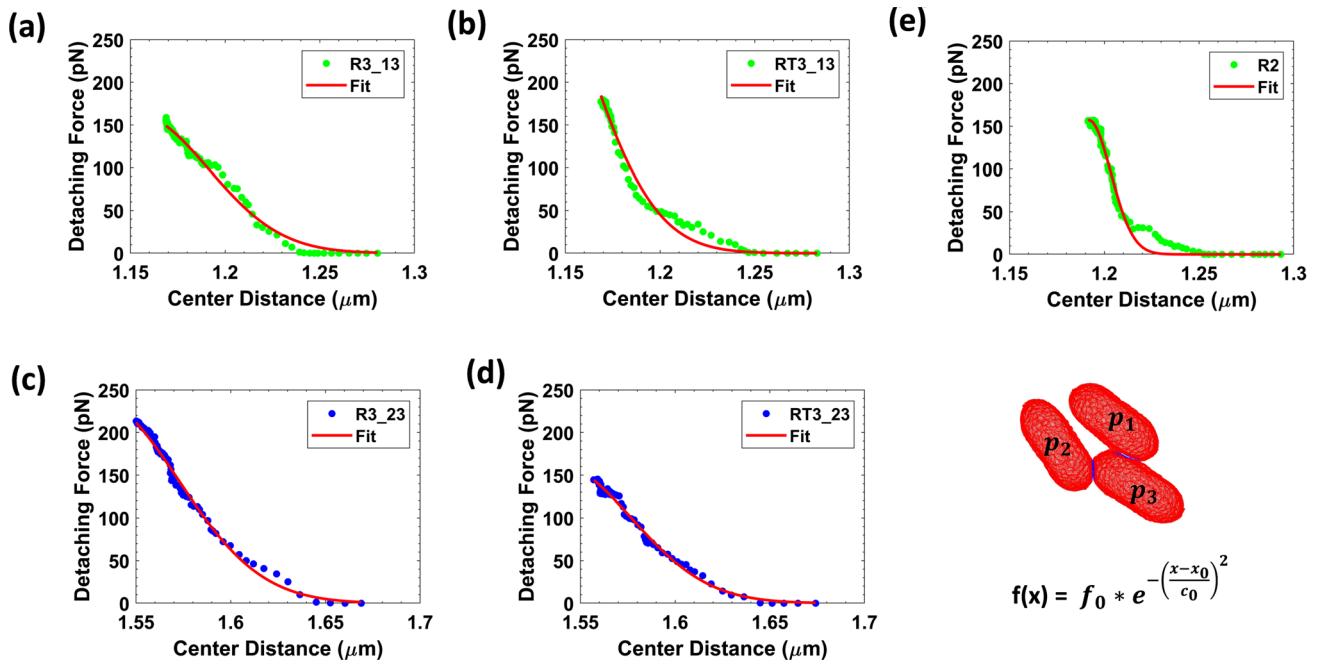


Fig. 9 Detaching force vs. center distance for **a** platelets p_1 and p_3 for the R3 setup, **b** platelets p_1 and p_3 for the RT3 setup, **c** platelets p_2 and p_3 for the R3 setup, **d** platelets p_2 and p_3 for the RT3 setup, **e** platelets p_1 and p_3 for the R2 setup

pseudopod formation (Maxwell et al. 2007), and $\alpha_{IIb}\beta_3$ -Fg interactions are well characterized under these flow conditions. Our group has modeled pseudopodia formation (Pothapragada et al. 2015) in the past and it can be integrated in the current model to study aggregation between activated platelets with changing morphology while using adaptive time stepping (Han et al. 2021; Zhang et al. 2015) to expand the range of simulated shear stresses in future multiscale models.

In conclusion, we present a multiscale multiple platelet aggregation framework that can analyze the aggregation dynamics, at molecular resolutions, to elucidate the macroscale stress and velocity distribution of the platelet membrane on the aggregate. Extending this framework to include more platelets under diverse shear flow conditions may help analyze the dynamics of platelet aggregation mediated by integrin $\alpha_{IIb}\beta_3$ and design potential pharmacological approaches to destabilize aggregates, thus preventing clot formation.

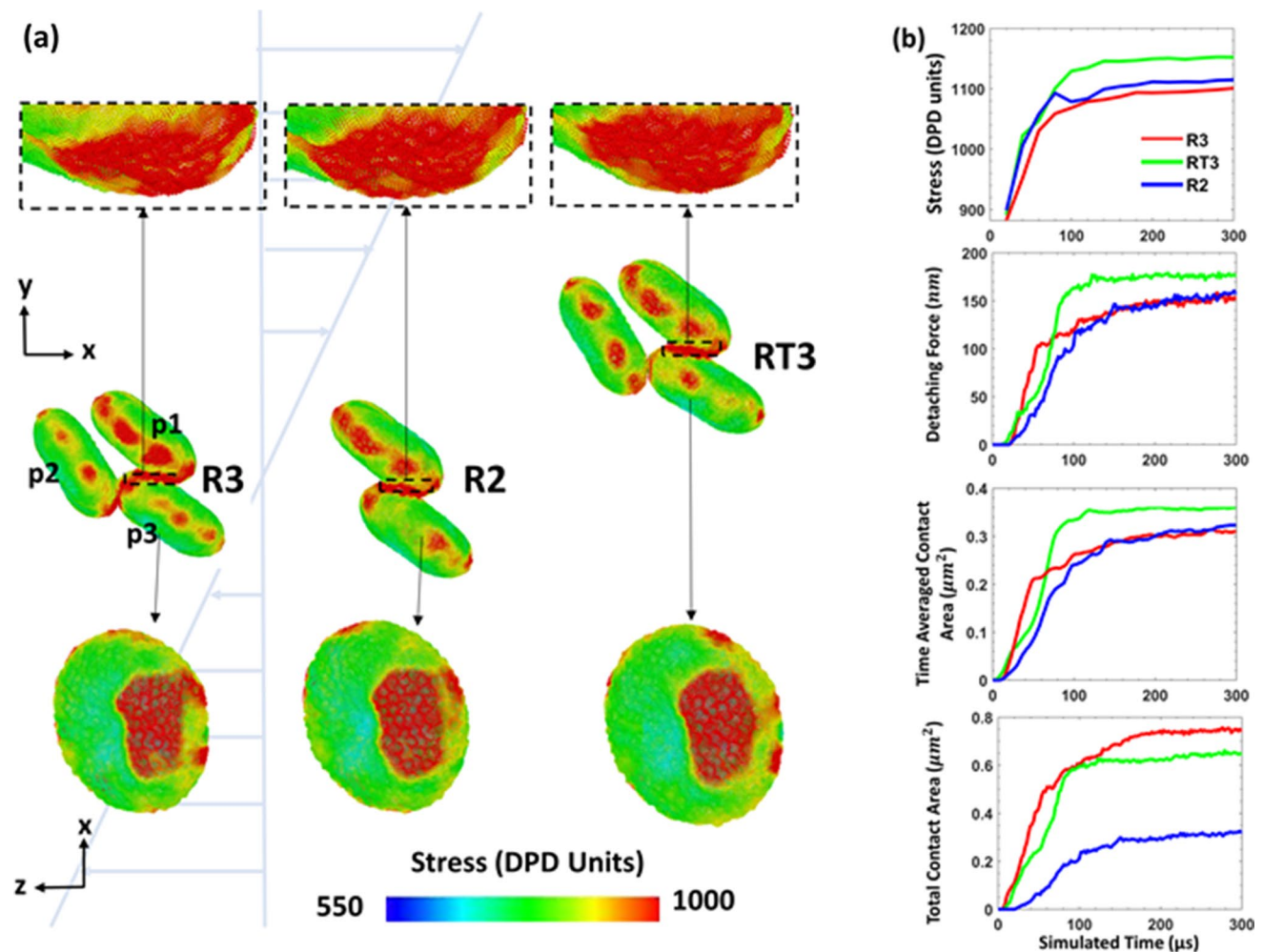


Fig. 10 (a) Comparison of stress for the R3, R2 and RT3 setups. The top row presents stress on p1, and the bottom row presents stress on p3 in the contact region represented by a_{13} (between platelets p1 and

p3) for R3, RT3 and R2. (b) Comparison of aggregation properties and stress in contact region for R3, RT3 and R2

Supplementary Information The online version of this article (<https://doi.org/10.1007/s10237-021-01428-6>) contains supplementary material, which is available to authorized users.

Funding This work, including the computer simulations, is made possible by grants from the National Institutes of Health (NIH) U01 HL131052-05 (PI: Danny Bluestein, Co-Is: Y. Deng and M. J. Slepian) and from the National Science Foundation grant 1531492 (PIs: R. Harrison and Y. Deng) funding access of the Seawulf supercomputer at the Institute for Advanced Computational Science at Stony Brook University.

Declaration

Conflicts of interest Prachi Gupta, Peng Zhang, Jawaad Sheriff, Danny Bluestein and Yuefan Deng declare that they have no conflict of interest.

References

- Alemu Y, Bluestein D (2007) Flow-induced platelet activation and damage accumulation in a mechanical heart valve: numerical studies. *Artif Organs* 31:677–688. <https://doi.org/10.1111/j.1525-1594.2007.00446.x>
- Apel J, Paul R, Klaus S, Siess T, Reul H (2001) Assessment of hemolysis related quantities in a microaxial blood pump by computational fluid dynamics. *Artif Organs* 25:341–347
- Benjamin EJ et al. (2019) Heart disease and stroke statistics-2019 update: a report from the American Heart association circulation 139:e56–e528. Doi: <https://doi.org/10.1161/CIR.0000000000000659>
- Brass LF, Diamond SL (2016) Transport physics and biorheology in the setting of hemostasis and thrombosis. *J Thromb Haemost* 14:906–917. <https://doi.org/10.1111/jth.13280>
- De Lazzari C, Darowski M, Ferrari G, Clemente F (1998) The influence of left ventricle assist device and ventilatory support on energy-related cardiovascular variables. *Med Eng Phys* 20:83–91

- Espanol P, Warren P (1995) Statistical mechanics of dissipative particle dynamics EPL. *Europhys Lett* 30:191
- Falk E (1985) Unstable angina with fatal outcome: dynamic coronary thrombosis leading to infarction and/or sudden death. Autopsy evidence of recurrent mural thrombosis with peripheral embolization culminating in total vascular occlusion. *Circulation* 71:699–708. <https://doi.org/10.1161/01.cir.71.4.699>
- Fedosov DA, Karniadakis GE (2009) Triple-decker: interfacing atomistic-mesoscopic-continuum flow regimes. *J Comput Phys* 228:1157–1171. <https://doi.org/10.1016/j.jcp.2008.10.024>
- Gao C, Zhang P, Marom G, Deng YF, Bluestein D (2017) Reducing the effects of compressibility in DPD-based blood flow simulations through severe stenotic microchannels. *J Comput Phys* 335:812–827. <https://doi.org/10.1016/j.jcp.2017.01.062>
- Goldsmith HL, McIntosh FA, Shahin J, Frojmovic MM (2000) Time and force dependence of the rupture of glycoprotein IIb-IIIa-fibrinogen bonds between latex spheres. *Biophys J* 78:1195–1206. [https://doi.org/10.1016/S0006-3495\(00\)76677-X](https://doi.org/10.1016/S0006-3495(00)76677-X)
- Groot RD, Warren PB (1997) Dissipative particle dynamics: bridging the gap between atomistic and mesoscopic simulation. *J Chem Phys* 107:4423–4435
- Guezuraga RM, Steinbring DY (2004) View from industry. *Eur J Cardiothorac Surg* 26 Suppl 1:S19–23; discussion S23–16
- Gupta P, Zhang P, Sheriff J, Bluestein D, Deng Y (2019) A multiscale model for recruitment aggregation of platelets by correlating with in vitro results. *Cell Mol Bioeng* 12:327–343. <https://doi.org/10.1007/s12195-019-00583-2>
- Haga JH, Beaudoin AJ, White JG, Strony J (1998) Quantification of the passive mechanical properties of the resting platelet. *Ann Biomed Eng* 26:268–277. <https://doi.org/10.1114/1.118>
- Han C, Zhang P, Bluestein D, Cong G, Deng Y (2021) Artificial intelligence for accelerating time integrations in multiscale modeling. *J Comput Phys* 427:110053. <https://doi.org/10.1016/j.jcp.2020.110053>
- Harker LA, Slichter SJ (1970) Studies of platelet and fibrinogen kinetics in patients with prosthetic heart valves. *N Engl J Med* 283:1302–1305. <https://doi.org/10.1056/NEJM197012102832402>
- Hartwig JH, Desisto M (1991) The cytoskeleton of the resting human blood-platelet - structure of the membrane skeleton and its attachment to actin-filaments. *J Cell Biol* 112:407–425. <https://doi.org/10.1083/jcb.112.3.407>
- Heinz H, Paul W, Binder K (2005) Calculation of local pressure tensors in systems with many-body interactions. *Phys Rev E Stat Nonlin Soft Matter Phys* 72:066704. <https://doi.org/10.1103/PhysRevE.72.066704>
- Jackson SP (2007) The growing complexity of platelet aggregation. *Blood* 109:5087–5095. <https://doi.org/10.1182/blood-2006-12-027698>
- Jackson SP, Nesbitt WS, Westein E (2009) Dynamics of platelet thrombus formation. *J Thromb Haemost* 7(Suppl 1):17–20. <https://doi.org/10.1111/j.1538-7836.2009.03401.x>
- Lakes R (2001) Materials science: a broader view of membranes. *Nature* 414:503–504
- Liang XM, Han SJ, Reems JA, Gao D, Sniadecki NJ (2010) Platelet retraction force measurements using flexible post force sensors. *Lab Chip* 10:991–998. <https://doi.org/10.1039/b918719g>
- Litvinov RI, Farrell DH, Weisel JW, Bennett JS (2016) The platelet integrin alphaIIb beta3 differentially interacts with fibrin versus fibrinogen. *J Biol Chem* 291:7858–7867. <https://doi.org/10.1074/jbc.M115.706861>
- Los DA, Murata N (2004) Membrane fluidity and its roles in the perception of environmental signals. *Biochim Biophys Acta* 1666:142–157. <https://doi.org/10.1016/j.bbame.2004.08.002>
- Maxwell MJ, Westein E, Nesbitt WS, Giuliano S, Doppeide SM, Jackson SP (2007) Identification of a 2-stage platelet aggregation process mediating shear-dependent thrombus formation. *Blood* 109:566–576. <https://doi.org/10.1182/blood-2006-07-028282>
- Michelson AD (2013) Platelets (Third Edition). Academic Press, Platelets (Third Edition)
- Mody NA, King MR (2008a) Platelet adhesive dynamics. Part I: characterization of platelet hydrodynamic collisions and wall effects. *Biophys J* 95:2539–2555. <https://doi.org/10.1529/biophysj.107.127670>
- Mody NA, King MR (2008b) Platelet adhesive dynamics. Part II: high shear-induced transient aggregation via GPIIb/IIIa-GPIIb/IIIa bridging. *Biophys J* 95:2556–2574. <https://doi.org/10.1529/biophysj.107.128520>
- Nesbitt WS et al. (2009) A shear gradient-dependent platelet aggregation mechanism drives thrombus formation. *Nat Med*. 15:665–673. http://www.nature.com/nm/journal/v15/n6/suppinfo/nm.1955_S1.html
- Obrien JR (1990) Shear-induced platelet-aggregation. *Lancet* 335:711–713
- Obrien JR, Salmon GP (1989) An independent hemostatic mechanism - shear induced platelet-aggregation. *Thrombosis Haemostasis* 62:258–258
- Parise LV, Phillips DR (1985) Reconstitution of the purified platelet fibrinogen receptor. Fibrinogen binding properties of the glycoprotein IIb-IIIa complex. *J Biol Chem* 260:10698–10707
- Pivkin IV, Richardson PD, Karniadakis G (2006) Blood flow velocity effects and role of activation delay time on growth and form of platelet thrombi. *Proc Natl Acad Sci USA* 103:17164–17169. <https://doi.org/10.1073/pnas.0608546103>
- Plimpton S, Thompson A, Crozier P (2012) LAMMPS molecular dynamics simulator. <http://lammps.sandia.gov>.
- Pothapragada S, Zhang P, Sheriff J, Livelli M, Slepian MJ, Deng Y, Bluestein D (2015) A phenomenological particle-based platelet model for simulating filopodia formation during early activation. *Int J Numer Method Biomed Eng* 31:e02702. <https://doi.org/10.1002/cnm.2702>
- Qiu Y, Ciciliano J, Myers DR, Tran R, Lam WA (2015) Platelets and physics: How platelets “feel” and respond to their mechanical microenvironment. *Blood Rev* 29:377–386. <https://doi.org/10.1016/j.blre.2015.05.002>
- Sheriff J, Bluestein D (2019) Platelet dynamics in blood flow. In: *Dynamics of blood cell suspensions in microflows*. CRC Press, pp 215–256
- Shiozaki S, Takagi S, Goto S (2016) Prediction of Molecular Interaction between Platelet Glycoprotein Iba and von Willebrand Factor using molecular dynamics simulations. *J Atheroscler Thromb* 23:455–464. <https://doi.org/10.5551/jat.32458>
- Slepian MJ et al (2017) Shear-mediated platelet activation in the free flow: perspectives on the emerging spectrum of cell mechanobiological mechanisms mediating cardiovascular implant thrombosis. *J Biomech* 50:20–25. <https://doi.org/10.1016/j.jbiomech.2016.11.016>
- Soares JS, Gao C, Alemu Y, Slepian M, Bluestein D (2013) Simulation of platelets suspension flowing through a stenosis model using a dissipative particle dynamics approach. *Ann Biomed Eng* 41:2318–2333. <https://doi.org/10.1007/s10439-013-0829-z>
- Sweedo A, Wise LM, Sheriff J, Bluestein D, Purdy JG, Slepian MJ (2020) MCS hypershear modulates platelet membrane fluidity, lipid species, and is gender specific. *J Heart Lung Transplantation* 39:S147. <https://doi.org/10.1016/j.healun.2020.01.1075>
- Thompson AP, Plimpton SJ, Mattson W (2009) General formulation of pressure and stress tensor for arbitrary many-body interaction potentials under periodic boundary conditions. *J Chem Phys* 131:154107
- Tosenberger A, Ataullakhanov F, Bessonov N, Pantelev M, Tokarev A, Volpert V (2012a) Modelling of thrombus growth and growth

- stop in flow by the method of dissipative particle dynamics. Russian J Numer Anal Math Model 27:507–522
- Tosenberger A, Ataullakhanov F, Bessonov N, Panteleev M, Tokarev A, Volpert V (2012b) The role of platelets in blood coagulation during thrombus formation in flow HAL
- Watala C, Golanski J, Boncler MA, Pietrucha T, Gwozdziński K (1998) Membrane lipid fluidity of blood platelets: a common denominator that underlies the opposing actions of various agents that affect platelet activation in whole blood. Platelets 9:315–327. <https://doi.org/10.1080/09537109876564>
- Weisel JW, Nagaswami C, Vilaire G, Bennett JS (1992) Examination of the platelet membrane glycoprotein IIb-IIIa complex and its interaction with fibrinogen and other ligands by electron microscopy. J Biol Chem 267:16637–16643
- Willemsen SM, Hoefsloot HCJ, Iedema PD (2000) No-slip boundary condition in dissipative particle dynamics. Int J Mod Phys C 11:881–890
- Yazdani A, Li H, Humphrey JD, Karniadakis GE (2017) A general shear-dependent model for thrombus formation. PLoS Comput Biol 13:e1005291. <https://doi.org/10.1371/journal.pcbi.1005291>
- Yazdani A, Zhang P, Sheriff J, Slepian MJ, Deng Y, Bluestein D (2018) Multiscale Modeling of Blood Flow-Mediated Platelet Thrombosis. In: Andreoni W, Yip S (eds) Handbook of materials modeling: applications: current and emerging materials. Springer, Cham, pp 1–32. Doi: https://doi.org/10.1007/978-3-319-50257-1_69-1
- Zhang N, Zhang P, Kang W, Bluestein D, Deng Y (2014) Parameterizing the morse potential for coarse-grained modeling of blood plasma. J Comput Phys 257:726–736. <https://doi.org/10.1016/j.jcp.2013.09.040>
- Zhang P, Gao C, Zhang N, Slepian MJ, Deng YF, Bluestein D (2014) Multiscale particle-based modeling of flowing platelets in blood plasma using dissipative particle dynamics and coarse grained molecular dynamics cell. Mol Bioeng 7:552–574. <https://doi.org/10.1007/s12195-014-0356-5>
- Zhang P, Zhang L, Slepian MJ, Deng Y, Bluestein D (2017) A multiscale biomechanical model of platelets: Correlating with in-vitro results. J Biomech 50:26–33. <https://doi.org/10.1016/j.jbiomech.2016.11.019>
- Zhang P, Zhang N, Deng Y, Bluestein D (2015) A multiple time stepping algorithm for efficient multiscale modeling of platelets flowing in blood plasma. J Comput Phys 284:668–686. <https://doi.org/10.1016/j.jcp.2015.01.004>

Publisher's Note Springer Nature remains neutral with regard to jurisdictional claims in published maps and institutional affiliations.